JOURNAL OF CATALYSIS 146, 93–102 (1994)

Glucose Hydrogenation on Promoted Raney-Nickel Catalysts

P. Gallezot,*,[1] P. J. Cerino,*,[2] B. Blanc,* G. Flèche,† and P. Fuertes†

*Institut de Recherches sur la Catalyse, CNRS, 2 avenue Albert Einstein, 69626 Villeurbanne Cedex, France; and †Société Roquette Frères, 62136 Lestrem, France

Received February 26, 1993; revised August 27, 1993

Glucose hydrogenation has been studied in a well stirred, high-pressure batch reactor on promoted Raney-nickel catalysts. Mo-, Cr-, and Fe-promoted catalysts were prepared by soda attack on $Ni_{40-x}Al_{60}M_x$ alloys. Sn-promoted catalysts were obtained by controlled surface reaction of $Sn(Bu)_4$ on the hydrogen-covered surface of a Raney-nickel obtained from a Ni_2Al_3 alloy. The loading of tin is stoichiometric and its distribution on the nickel surface is very homogeneous down to nanometer scale. For an optimum promoter concentration the catalysts are up to seven times more active than unpromoted ones. A good distribution of the promoter in the catalyst grain is required to obtain the best rate enhancement; in the case of molybdenum this is obtained by annealing the alloys. The promoters in a low-valent state on the nickel surface act as Lewis adsorption sites for the oxygen atom of the carbonyl group which is then polarized and thus more easily hydrogenated via a nucleophilic attack on the carbon atom by hydride ions. The activities of Mo- and Cr-promoted catalysts decrease slightly after several recyclings in successive hydrogenation experiments. This is mostly due to surface poisoning by cracking products formed in side reactions. Fe- and Sn-promoted Raney-nickel catalysts deactivate very rapidly because Fe and Sn are leached away from the surface. Iron is washed to the liquid phase whereas tin remains in the Raney-nickel micropores.

INTRODUCTION

The catalytic hydrogenation of glucose (d-glucose or dextrose) accounts for an annual production of ca. 500,000 tons of sorbitol, a valuable polyol used as additives in foods, drugs, and cosmetics or as a synthon for the preparation of various chemicals, including vitamin C. This catalytic process of growing economic importance is conducted mainly on Raney-nickel catalysts promoted with metals which improve their activities, selectivities, and stabilities. Metal promoters are usually incorporated into Raney precursor alloys (1, 2), typically 0.5 to 5 mol% of one or two metals being added to a nickel–aluminum melt. The resulting alloy is then leached with concentrated alkali solutions to remove part of the aluminum, thus yielding highly porous, tri- or polymetallic Raney-nickel catalysts. Molybdenum (3, 4), tin (5), chromium (4, 6), iron (4, 7), and titanium (6, 8) among other metals have been used to enhance the activity of Raney-nickel catalysts in glucose hydrogenation.

We started a series of investigations to better understand how metal promoters modify the activity of catalysts in the hydrogenation of hexoses. Since these catalysts are recycled many times in industrial operations, their stabilities after repeated recycling have been studied as a function of the nature and amounts of a metal promoter M, in well-characterized catalysts. Chromium-, molybdenum-, and iron-promoted catalysts were prepared by soda attack on $Ni_{40-x}Al_{60}M_x$ alloys whereas tin-promoted catalysts were obtained by controlled surface reaction of tetrabutyl tin on a Raney-nickel catalyst derived from a $Ni_{40}Al_{60}$ alloy. Metal loading via surface reaction was used earlier to prepare Pt–Sn (9), Rh–Sn (10), and Ni–Sn (11, 12) supported bimetallic catalysts and was also applied to deposit tin on Raney-nickel catalysts (13, 14). A preliminary report on glucose hydrogenation data has been published previously (15).

EXPERIMENTAL

Catalyst preparation. Precursor alloys were prepared in a metallurgical research center (Imphy SA, France) by melting in an induction furnace high-purity nickel, aluminum and a third metal in required amounts to obtain the composition $Ni_{40-x}Al_{60}M_x$ (M = Cr, Mo, Fe). The melt was cast into a crucible to form 1-kg ingots. All these operations were carried out in argon atmosphere to avoid metal oxidation. In some cases, the ingots were annealed for 3 weeks at 1223 K under argon to improve further the homogeneity of the solid solution of metal M in the Ni_2Al_3 lattice.

The ingots were crushed into fragments which were subsequently ground with a hammer-mill to obtain a fine powder which was sieved to collect only grains smaller than 40 μm. The alloy powder in 100 g batch was leached

[1] To whom correspondence should be addressed.

[2] Present address: Shell France, 92564 Rueil-Malmaison, France.

0021-9517/94 $6.00

TABLE 1

Composition of Precursor Alloys and Catalysts

Catalysts	Composition of precursor alloy[a]		Composition of fresh catalysts[b]					Composition of used catalysts[a]	
	Al/Ni	M/Ni($\times 10^3$)	Ni	Al	M	Al/Ni	M/Ni($\times 10^3$)	Al/Ni	M/Ni($\times 10^3$)
RNi	1.56		90.6	9.1		0.22		0.22	
RNiFe1	1.62	55	81.5	12.7	4.55	0.34	59	0.29	42
RNiFe2	1.63	120	74.3	13.5	8.22	0.39	116		
RNiFe3	1.68	185	69.8	14.6	12.3	0.45	186	0.34	68
RNiFe4	1.89	251	62.7	15.1	15.9	0.52	267	0.37	103
RNiSn1[c]			82.8	8.7	2.73	0.22	16(16)[d]	0.20	16
RNiSn2[c]			80.5	8.3	5.00	0.22	31(31)[d]	0.20	29
RNiSn3[c]			78.1	8.2	9.05	0.22	57(63)[d]	0.20	58
RNiMo1	1.55	12	83.4	11.4	0.55	0.30	4		
RNiMo2	1.59	26	84.2	11.6	1.24	0.30	9		
RNiMo1[e]	1.57	13	90.1	9.6	0.68	0.22	5		
RNiMo2[e]	1.59	26	87.7	9.2	1.28	0.25	9		
RNiCr1	1.55	13	82.1	10.0	0.94	0.34	13		
RNiCr2	1.57	22	83.4	13.5	1.76	0.35	24		
RNiCr3	1.70	116	69.8	17.4	6.82	0.65	110		
RNiCR1[e]	1.55	14	83.6	10.6	0.99	0.28	13		
RNiCr2[e]	1.58	25	82.3	10.5	1.89	0.28	26		
RInd[f]						0.13	10		

[a] Molar ratio.
[b] Weight percent.
[c] Prepared from RNi by controlled surface reaction with tetrabutyl tin.
[d] Expected M/Ni ratios in parentheses.
[e] Precursor alloys annealed at 1223 K for 3 weeks.
[f] Commercial catalyst containing molybdenum.

with a concentrated soda solution (500 cm^3, 6 mol $liter^{-1}$) added slowly at room temperature. Then, the suspension was refluxed for 2 h, decanted and washed with soda (1 mol $liter^{-1}$). The powder was submitted to three successive refluxing treatments in 6, 4, and 2 mol $liter^{-1}$) soda solutions and finally kept under soda (1 mol $liter^{-1}$). The nomenclature and compositions of the catalysts and of the precursor alloys are given in Table 1.

Catalysts promoted with tin were prepared by controlled surface reaction of terabutyl tin with hydrogen adsorbed on the surface of RNi, an unpromoted catalyst obtained by soda attack on a $Ni_{40}Al_{60}$ alloy. The surface reaction was carried out entirely in the liquid phase. The RNi powder was stirred successively in water, ethanol, ethyl acetate and n-heptane. Then, the *n*-heptane suspension was stirred in a Teflon-lined autoclave which was pressurized under 4 MPa H_2-pressure and heated at 333 K for 1 h. Then, required amounts of $Sn(C_4H_9)_4$ in *n*-heptane were introduced under H_2-pressure in the autoclave and the suspension was stirred for 2 h under 4 MPa of H_2 at 333 K. After depressurization and purging under N_2 the catalyst suspension was decanted and rinsed successively with *n*-heptane, ethyl acetate, ethanol and water. The compositions of the catalysts are given in Table 1.

Catalyst characterization. The compositions of alloys and catalysts were determined by atomic absorption spectrophotometry after total dissolution in acidic solutions. Their structure was studied by X-ray diffraction with a powder diffractometer, the catalyst powder being kept wet under a sealed, X-ray-transparent window to avoid oxidation by air. The average size of nickel crystallites was determined from the integral width of the (111) nickel reflection using the Scherrer equation after correcting for instrumental broadening with the Warren procedure (16). Since the profile of the (111) reflection is perturbed at high Bragg angles by the (200) reflection, the linewidth analysis was done over the low-angle half-profile. Adsorption–desorption measurements of nitrogen at 77 K were performed by volumetry with an automated sorptometer. Before measurements catalysts were outgassed under reduced pressure firstly at 298 K for 1 h then at 393 K for 4 h to avoid any oxidation and/or sintering of Raney-nickel. Surface areas were determined from the BET transform and pore distributions were calculated from the nitrogen adsorption isotherm with a model of cylindrical pores.

The morphology of the catalyst was studied by transmission electron microscopy (TEM) with a JEOL 100CX

microscope. Thin sections of the catalyst grains were cut with a diamond-knife ultramicrotome after embedding in epoxy resin. To protect the catalyst from oxidation, the sections floating on water were picked up with a carbon-coated copper grid and kept under a drop of water which evaporated under vacuum in the airlock of the microscope. The local composition of catalyst grains was studied on the thin sections using a field-emission gun, scanning transmission electron microscope (STEM) equipped with an energy dispersive X-ray emission analyzer (EDX). The spatial resolution of analysis was 1.5 nm. The thermodesorption measurements used to determine the volume of hydrogen chemisorbed on the metal and the magnetic measurements to determine the saturation magnetization were described previously (17). The fresh catalysts prepared by soda attack were stocked for one week prior to the hydrogen thermodesorption measurements. The metal area was calculated from the total volume of H_2 thermosorbed from fresh catalysts assuming an equal distribution of atoms among the (100), (110), and (111) planes and a stoichiometry H/Ni = 1.

Catalytic hydrogenation procedure. Eighty g of glucose monohydrate were dissolved at 333 K in 120 g of distilled water resulting in a 175-ml, 2.31 mol liter^{-1} solution. This solution, together with 1.6 g of Raney-nickel previously water-washed until neutral, was poured into a 500-ml Teflon-lined autoclave. The pH of the suspension was adjusted to 6.5 with a 10% solution of acetic acid. The autoclave was purged with helium and pressurized under 4.5 MPa of hydrogen. The temperature was increased from 333 to 403 K and the reaction started after pressurization at 5 MPa and stirring at 1400 rpm. Samples of the reaction medium were taken periodically for HPLC analysis. Reaction kinetics were also followed by the pressure drop in a hydrogen reserve feeding the autoclave through a constant pressure valve. After the first hydrogenation had been completed the catalyst was magnetically trapped at the bottom of the vessel and the liquid was purged. Then the catalyst was washed with distilled water, magnetically decanted and after a second purge a fresh solution of glucose was loaded. All these steps were conducted under high hydrogen pressure. The second hydrogenation was carried out under the same conditions and the whole process was repeated until the fifth hydrogenation was completed. The HPLC analysis was performed with a Shimadzu pump (LC9A) and refractometer (RID-6A). Separation of the polyols (glucose, fructose, mannitol, sorbitol) was achieved with an Aminex HPX-87C column from Bio-Rad.

RESULTS AND DISCUSSION

1. Preliminary Study of Reaction Kinetics

Preliminary rate measurements were performed on RNi Ind, a commercial catalyst promoted with molybdenum

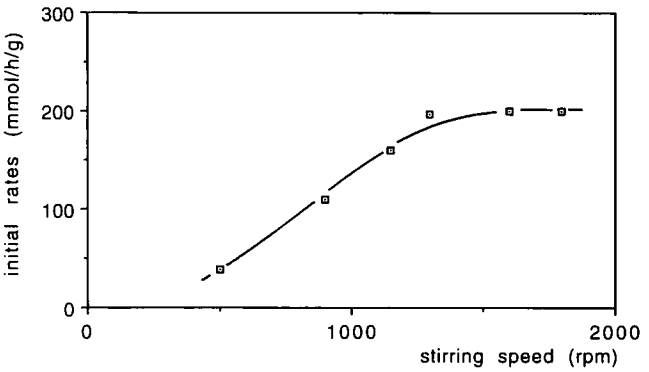

FIG. 1. Initial rates of glucose hydrogenation vs stirring speed.

(Table 1). The initial rates of reaction were obtained from the initial slope of the curves giving the amount of converted glucose as a function of time.

First, the dependence of the rate upon the stirring speed was studied. Figure 1 shows that there is a plateau above 1200 rpm where the rate does not depend upon the stirring speed; a standard stirring speed of 1400 rpm was used subsequently.

Figure 2 shows in agreement with previous studies on glucose hydrogenation (18–20) that the reaction rate is proportional to the mass of catalyst in a very large range up to 6 wt% of catalyst with respect to glucose; in our standard reaction conditions 2 wt% of catalyst was used. This is a clear indication for the absence of external mass transfer limitation but it does not rule out possible diffusional limitation in the micropores of Raney-nickel grains. However, it was concluded from a calculation performed for glucose hydrogenation under similar conditions on Raney-nickel catalysts of comparable pore size and grain size that there is no diffusional limitation in pores (21). The activation energy deduced from the Arrhenius plot corresponding to the 348–428 K temperature range was 26.7 kJ mol^{-1}.

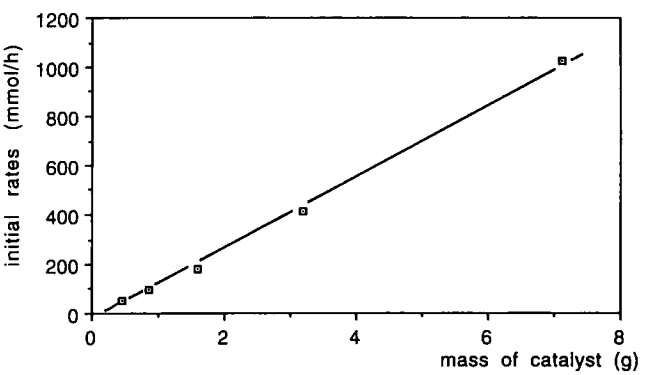

FIG. 2. Initial rates of glucose hydrogenation vs mass of catalyst.

TABLE 2

Texture Parameters and Initial Rates in Successive Hydrogenations

Catalyst	BET area ($m^2 g^{-1}$)		Crystallite size (nm)		Metal area ($m^2 g^{-1}$)	Initial rates						
						1		2	3	4	5	
	[a]	[b]	[a]	[b]		[c]	[d]	[c]	[c]	[c]	[c]	[d]
RNi	77	64	4.3	4.7	106	68	0.88	68	68	56	50	0.78
RNiCr1						350		300	293	287	250	
RNiCr2	100	69	3.6	4.0	146	375	3.75	350	318	293	275	3.90
RNiCr3						84		58	36			
RNiCr2[e]						350		331	318	293		
RNiMo1	79					243		206	187	175	156	
RNiMo2	83	59	3.7	4.1	113	262	3.15	237	231	187	175	2.97
RNiMo2[e]						431		281	225	218	212	
RNiInd						231		181	156	137	125	
RNiFe1	86	65	3.6	3.7		106	1.23	93	68	62	60	0.92
RNiFe2	90					287	3.19	187	125	106	88	
RNiFe3	97	75				575	5.92	312	181	143	113	1.51
RNiFe4	80					406	5.07	262	150	131	119	
RNiSn1	63	55			91	213	3.38	112	51			
RNiSn2	70	48			41	289	4.13	144	48			
RNiSn3	53	49			29	349	6.58	121	22			

[a] Fresh catalyst.
[b] After the fifth hydrogenation.
[c] In mmol $h^{-1} g^{-1}$.
[d] In mmol $h^{-1} m^{-2}$ (calculated from the BET area).
[e] Derived from precursor alloys annealed at 1223 K for 3 weeks.

2. *Unpromoted Catalyst*

The precursor alloy of catalyst RNi has the required Ni_2Al_3 composition within 1% (Table 1). The X-ray diffraction pattern taken on the powdered alloy exhibits only the Bragg reflections corresponding to the Ni_2Al_3 cubic lattice. The texture parameters of the RNi catalyst derived from the Ni_2Al_3 ground alloy are given in Table 2. The metal area estimated from the amount of hydrogen thermodesorbed from the fresh catalyst is 106 $m^2 g^{-1}$, i.e., 40% larger than the BET area. A similar discrepancy, also observed for the other promoted catalysts (Table 2), was reported previously (17) and attributed to the presence of very small pores (<1 nm) which would be accessible to hydrogen but not to nitrogen. However, this could be due to the presence of residual molecules of water which react with nickel during the thermodesorption treatment to give hydrogen.

After five hydrogenation runs, there is no change in the Al/Ni ratio, which indicates that no aluminum is leached away during reaction; however, the BET area decreases from 77 to 64 $m^2 g^{-1}$. This could be attributed to a partial sintering of the metal; indeed, the average crystallite size measured by X-ray line broadening increases from 4.3 to 4.7 nm (Table 2) but this is not sufficient to account for the decrease of the BET area. Most probably the BET area of the used catalyst is underestimated because of the presence in the catalyst micropores of organic residues which cannot be washed out or outgassed and which decrease the amount of physisorbed nitrogen.

The catalytic activity after five hydrogenation runs decreases by 26% (Table 2). The loss of activity is due in part to a weak sintering of the catalyst grains which reduces the active area but the main cause of deactivation is the presence of organic molecules poisoning the nickel surface. These strongly adsorbed species could be cracking products of glucose or sorbitol or other products formed in side reaction. Thus, small amounts of gluconic acid formed by the Cannizzaro reaction on hydroxyl groups still present in deep narrow pores would be sufficient to account for the deactivation since carboxylic acids are strongly bonded to nickel (22).

The poisoning of the nickel surface is confirmed by measurements of the saturation magnetization. It decreases from 24.4 to 20.5 G $cm^3 g^{-1}$ after five hydrogenations. According to Selwood (23), this means that a fraction of the surface nickel atoms are demagnetized because of strong bonding interactions with adsorbed species.

3. *Chromium-Promoted Catalysts*

The X-ray pattern of chromium-containing, precursor alloys of catalysts RNiCr1 and RNiCr2, either as such or

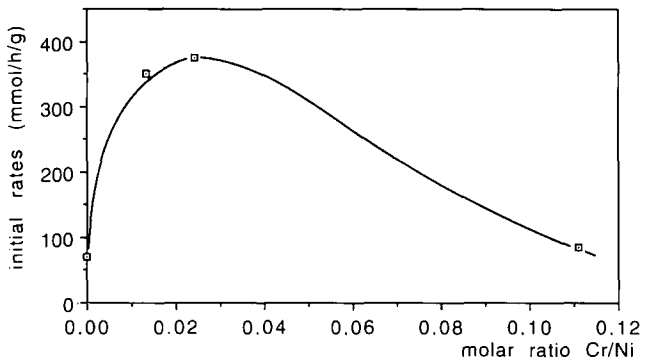

FIG. 3. Initial rates of glucose hydrogenation of Cr-promoted catalyst vs the molar ratio Cr/Ni in the catalyst.

after an annealing treatment, show only the Bragg reflections corresponding to the Ni_2Al_3 phase, which means that Cr-atoms substitute for Ni atoms in the Ni_2Al_3 phase. This is in agreement with the ternary phase diagram of Kaufman and Nesor (24), showing that chromium is soluble in Ni_2Al_3 up to 2 mol%. On the other hand, the pattern of the precursor alloy of RNiCr3 shows, in addition to the peaks from Ni_2Al_3, small reflections corresponding to other phases such as Al_9Cr_4.

The soda attack leaves a larger percentage of aluminum than in RNi and does not change significantly the Cr/Ni ratio, which means that chromium is not leached away with aluminum and therefore is well associated with nickel.

The metal dispersion is higher than in the unpromoted catalyst. Thus in RNiCr2 the BET area and the metal area are 30 and 35% larger respectively than in RNi (Table 2). Accordingly, the crystallite sizes measured by X-ray line broadening are smaller (Table 2). The distribution of chromium and aluminum in the catalyst grains measured by STEM–EDX analysis is very homogeneous. Thus the ratios Cr/Ni or Al/Ni measured on ultramicrotome sections of RNiCr2 are constant whatever the zone analysed (edge center) and whatever the size of the area scanned in the range 10 nm^2 to 10 μm^2. The ratios are also constant from one grain to another and correspond to the nominal overall composition.

Table 2 gives the initial rates of glucose hydrogenation on the fresh, Cr-promoted catalysts. They are very active; for instance, RNiCr2 is 5.5 times more active than RNi. The promoting effect of chromium on carbonl group hydrogenation was observed earlier in glucose (4) and acetophenone (25) hydrogenation. Figure 3 shows that there is an optimum concentration at 1.76 wt% Cr (RNiCr2), larger loadings resulting in a drop of activity. Several factors could account for rate enhancement. First, Cr-promoted catalysts have larger active areas. However, the BET area and the metal area are only 30 and 35% larger respectively in RNiCr2 than in RNi which cannot account for the 550% rate enhancement. Second, the higher activity could be attributed to the higher amounts of residual aluminum in the promoted catalysts; this interpretation has been given in the case of glucose (4) and acetone hydrogenation (2). In contrast, an inhibiting effect of residual aluminum was reported in acetophenone hydrogenation (25). Our data show that there is no correlation between the activities and the aluminum contents in these catalysts as well as in catalysts promoted with molybdenum (vide infra). Furthermore, the loading of tin promoters via organometallic compounds boosts the activity without changing the aluminum concentration (vide infra).

To interpret the effect of chromium we suggest a concerted mechanism of activation and hydrogenation of the carbonyl function which involves the association on the catalyst surface of reduced nickel atoms and low-valent chromium ions. It has been shown by XPS that chromium at the surface of Raney nickel is in the oxidation state Cr^{III} (26). Under reaction conditions chromium should be in the Cr^{III} state, which is the thermodynamically stable species in water at pH = 7 and at -0.62 V, the potential of the hydrogen electrode taken by the metal under the present reaction conditions. Let us assume that the pyranic form of glucose is in fast equilibrium with the linear form. The Cr^{III} species on the surface can act as Lewis adsorption sites, the glucose molecule being adsorbed via the donation of a lone electron pair from the oxygen of the carbonyl group. This bonding polarizes the C=O bond which favors a nucleophilic attack on the carbon atom by hydrogen dissociated on neighboring nickel atoms. This mechanism requires the presence of both Ni–H and Cr^{III} species on the surface and the maximum of activity should correspond to an optimum surface concentration of Cr^{III}. A larger concentration is detrimental to the activity because too many surface nickel atoms are covered by Cr^{III} species. Note that chromium atoms possibly located underneath the surface would also be beneficial because they would transfer electrons toward nickel surface atoms, thus easing the formation of H^- species participating in the nucleophilic attack on the carbon atom of the polarized carbonyl group.

Table 2 gives the initial rates of glucose hydrogenation on chromium-promoted catalysts in successive hydrogenation runs on the same catalyst. The total drop of activity of RNiCr2 after five recyclings is 27% compared to 28% for RNiCr1 containing twice as little chromium and to 26% for RNi containing no chromium. This loss of activity parallels roughly the loss of the BET area in the three samples. As discussed previously, the loss of BET area is mainly due to the presence of strongly adsorbed organic molecules in the micropores and the decrease of activity of RNi was also ascribed to organic residues poisoning

the Raney-nickel surface. It can be concluded that the concentration of chromium in these different catalysts does not play a major role on the main cause of deactivation in the present conditions, i.e., on side reactions leading to cracked products or to acids via the Cannizzaro reaction. However, under different reaction conditions (e.g., at higher temperatures) or after many recyclings, the promoter might well be useful to stabilize the texture of the Raney-nickel and thus to prevent deactivation by sintering.

4. *Molybdenum-Promoted Catalysts*

The X-ray pattern of the Mo-promoted alloys shows not only the reflections of the Ni_2Al_3 phase but extraneous phases such as Mo_3Al and Mo_3Al_8. This is in agreement with the ternary phase diagrams (24) indicating that the solubility of Mo in Ni_2Al_3 is very small. Table 1 giving the Mo/Ni ratio shows that up to 2/3 of molybdenum is leached away during the soda attack. This fraction probably corresponds to molybdenum incorporated in Mo–Al phases whereas most of the molybdenum associated with nickel should remain in the final catalyst. The Mo-promoted alloys have been annealed at 1223 K in argon for 3 weeks in an attempt to improve the homogeneity. This treatment does not decrease the fraction of molybdenum leached away during the soda attack (Table 1) but results in a better homogeneity of the distribution of promoter associated with nickel. To check this point, STEM–EDX analyses at high-spatial resolution have been performed on ultramicrotome sections of RNiMo2a. Occasionally, pockets containing pure molybdenum oxide were detected but otherwise the distribution of molybdenum is very homogeneous since constant Mo/Ni ratios were found throughout sections and from one grain to another. The effect of the annealing treatment on the activity and stability of the catalyst is conspicuous from the data given in Table 2. The initial rate of RNiMo2a is 65% larger than in RNiMo2 and it is higher than those of chromium-promoted catalysts. The catalyst deactivates faster during the first two hydrogenation runs but the activity is more stable and higher than in RNiMo2 during subsequent recyclings. In contrast, annealing treatments had no effect on chromium catalysts because the distribution of the metal promoters was homogeneous, probably as a result of the higher solubility of chromium in the Ni_2Al_3 phase.

The need for a good distribution of metal promoters in Raney-nickel grains to obtain high hydrogenation activities is well understood by the mechanism of rate enhancement proposed in the case of chromium catalysts. Indeed, this mechanism implies that electropositive metal promoters like chromium or molybdenum should be evenly distributed on the nickel surface in the form of low-valent species so that contiguous Ni–H and $M^{(+)}$ sites in optimum proportion activate in a concerted way the hydrogenation of the carbonyl group.

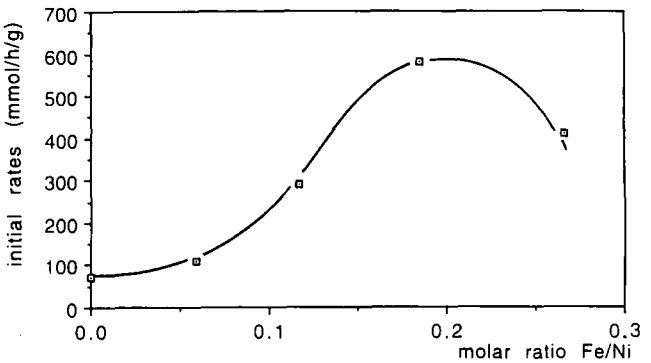

FIG. 4. Initial rates of glucose hydrogenation on fresh RNiFe catalyst vs Fe/Ni ratios.

Finally, it is noteworthy that most of the catalysts prepared in the laboratory are more active and stable than a molybdenum-promoted commercial catalyst (RNi Ind, Table 2) which was selected among the best catalysts for glucose hydrogenation.

5. *Iron-Promoted Catalysts*

The solubility of iron in the Ni_2Al_3 phase can be as high as 10 wt% (27), i.e., much higher than the solubility of Mo and Cr. $Ni_{40-x}Al_{60}Fe_x$ alloys were prepared with x = 2 to 8; their compositions are given in Table 1. The X-ray patterns of RNiFe1 and RNiFe2 alloys showed only the Bragg reflections of the Ni_2Al_3 cubic lattice but extraneous phases such as FeAl and Fe_2Al_5 were detected in RNiFe3 and RNiFe4 alloys. The soda attack does not produce any loss of iron since the Fe/Ni ratios are comparable in the alloy and in the corresponding catalysts (Table 1).

The rates of glucose hydrogenation are enhanced on Fe-promoted catalysts; thus RNiFe3 is 8.5 times more active than RNi (Table 2). Taking into account the larger BET area of RNiFe3, its activity per unit area is still 6.7 times that of RNi. The rate enhancement can be explained, as in the case of molybdenum and chromium promoters, by an activation of the C=O bond by low-valent iron atoms on the surface of nickel. However, Fig. 4 shows that the optimum concentration of iron is much higher than that of chromium (Fig. 3). Since we have checked by STEM-EDX that both metal promoters are homogeneously distributed in the Raney-nickel grains, the higher efficiency of chromium to promote the C=O bond activation at low concentration could be due to its higher electropositivity compared to iron. However, it is more probable that larger amounts of iron are needed because iron is rapidly leached from the surface (vide infra) so that the actual concentration of iron on the nickel

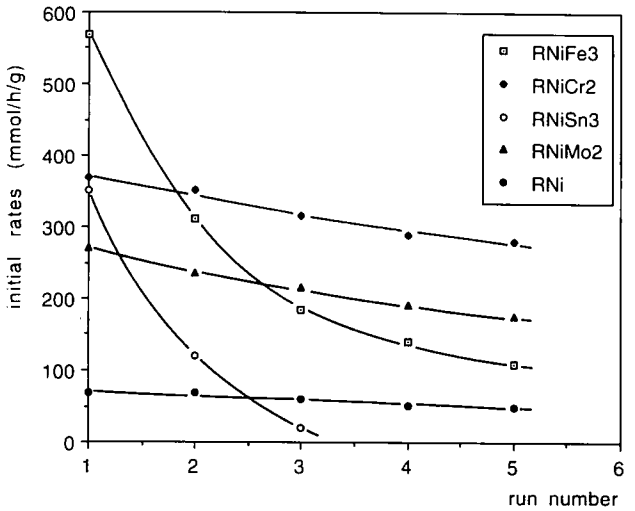

FIG. 5. Initial rates of glucose hydrogenation for different catalysts as a function of the number of recycling (1 corresponds to hydrogenation on the fresh catalyst).

surface, even in the first minutes of reaction, might be far below the nominal composition measured by chemical analysis or by STEM–EDX analysis on the fresh catalyst before reaction.

Table 2 gives the initial rates of hydrogenation after successive recycling of the Fe-promoted catalysts. They deactivate very rapidly especially when compared to Cr- and Mo-promoted catalysts (Fig. 5). The main cause of deactivation is well understood from the analytical data given in Table 1 showing that two-thirds of the iron atoms are leached away in the course of the five hydrogenation runs conducted on RNiFe3. This is the main cause of the 80% activity loss experienced by the catalyst. However, other causes such as those invoked to interpret the activity decay of Cr- and Mo-promoted catalysts, namely metal sintering and poisoning by strongly adsorbed cracking products, probably contribute to deactivate the catalyst further. The leaching of iron is well understood from the pH-potential diagram of iron showing that under the reaction conditions ferrous ions are the thermodynamically stable species.

6. *Tin-Promoted Catalysts*

6.1. Characterization of catalysts. Tin was loaded via controlled surface reaction of $Sn(Bu)_4$ with hydrogen adsorbed on the surface of catalyst RNi obtained by soda attack on Ni_2Al_3. Catalysts RNiSn1, RNiSn2, and RNiSn3 thus obtained were extensively characterized before and after three hydrogenation cycles. Table 1 shows that the Sn/Ni ratios measured on RNiSn1 and RNiSn2 are exactly those expected for a quantitative loading of $Sn(Bu)_4$ from the solution to the catalyst. For RNiSn3 up to 9 wt% of tin is fixed which corresponds to a surface reaction yield of 90%. According to previous work (14) the reaction of organometallic tin compounds with a nickel surface can be written

$$x\,\mathrm{NiH} + \mathrm{SnR}_n \longrightarrow \mathrm{Ni}_x\mathrm{SnR}_{n-x} + x\mathrm{RH}$$
$$\mathrm{Ni}_x\mathrm{SnR}_{n-x} + (n-x)/2\,\mathrm{H}_2 \longrightarrow \mathrm{Ni}_x\mathrm{Sn} + (n-x)\,\mathrm{RH}.$$

From this stoichiometric surface reaction one would expect a homogeneous distribution of tin on the Raney-nickel surface. To check this point a very detailed study of the RNiSn2 catalyst was performed by TEM and by STEM-EDX analysis at high resolution on ultramicrotome sections of the catalyst. Figures 6a and 6b give TEM views at different magnification of RNiSn2. The section is so thin that individual Ni-crystallites can be imaged, their sizes being mainly in the range 3–9 nm. The distribution of tin in the Raney-nickel grains was monitored by STEM–EDX analysis with the smallest electron-probe (5 Å) given by the field-emission gun of the VGHB501 microscope. Sections of different grains and different areas on a given section were analysed on the fresh catalyst. Except for occasional Sn-enrichment near the outer surface of grains, the Sn/Ni ratios are fairly constant and in good agreement with the overall catalyst composition. The amounts of hydrogen thermodesorbed from the fresh catalysts are given in Fig. 7. The larger the amount of tin, the smaller the amount of chemisorbed hydrogen. As in the case of Pt–Mo catalysts prepared by decomposition of $Mo(CO)_6$ on platinum (28), a lower H_2-chemisorption can be attributed to the coverage of the surface by the deposited adatoms. Indeed low-valent tin atoms on the surface would not adsorb hydrogen but would hinder the chemisorption on the underlying nickel atoms.

From the results of STEM–EDX and thermodesorption measurements on the fresh catalysts it can be concluded that tin is homogeneously distributed on the nickel surface. This is consistent with a preparation mode involving the reaction of $Sn(Bu)_4$ with surface hydrogen followed by a mild thermal treatment at 413 K which does not produce a migration of tin atoms from the surface into the bulk.

After three hydrogenation runs, analytical data (Table 1) show that there is no leaching of tin during reaction. Furthermore, STEM-EDX analysis of RNiSn2 shows that tin is still homogeneously distributed in the Raney-nickel grains. However, STEM-EDX measurements at high spatial resolution indicate that tin is now concentrated in the micropores. Thus, EDX analysis conducted with a 2-nm spatial resolution on Ni-crystallites such as those observed in Fig. 6b gives a Sn concentration three times smaller than in the space left between Ni-crystallites, i.e., in the micropores. The leaching of Sn from the surface of Ni-crystallites and the precipitation in the micropores can be inferred from the potential-pH diagram of tin which

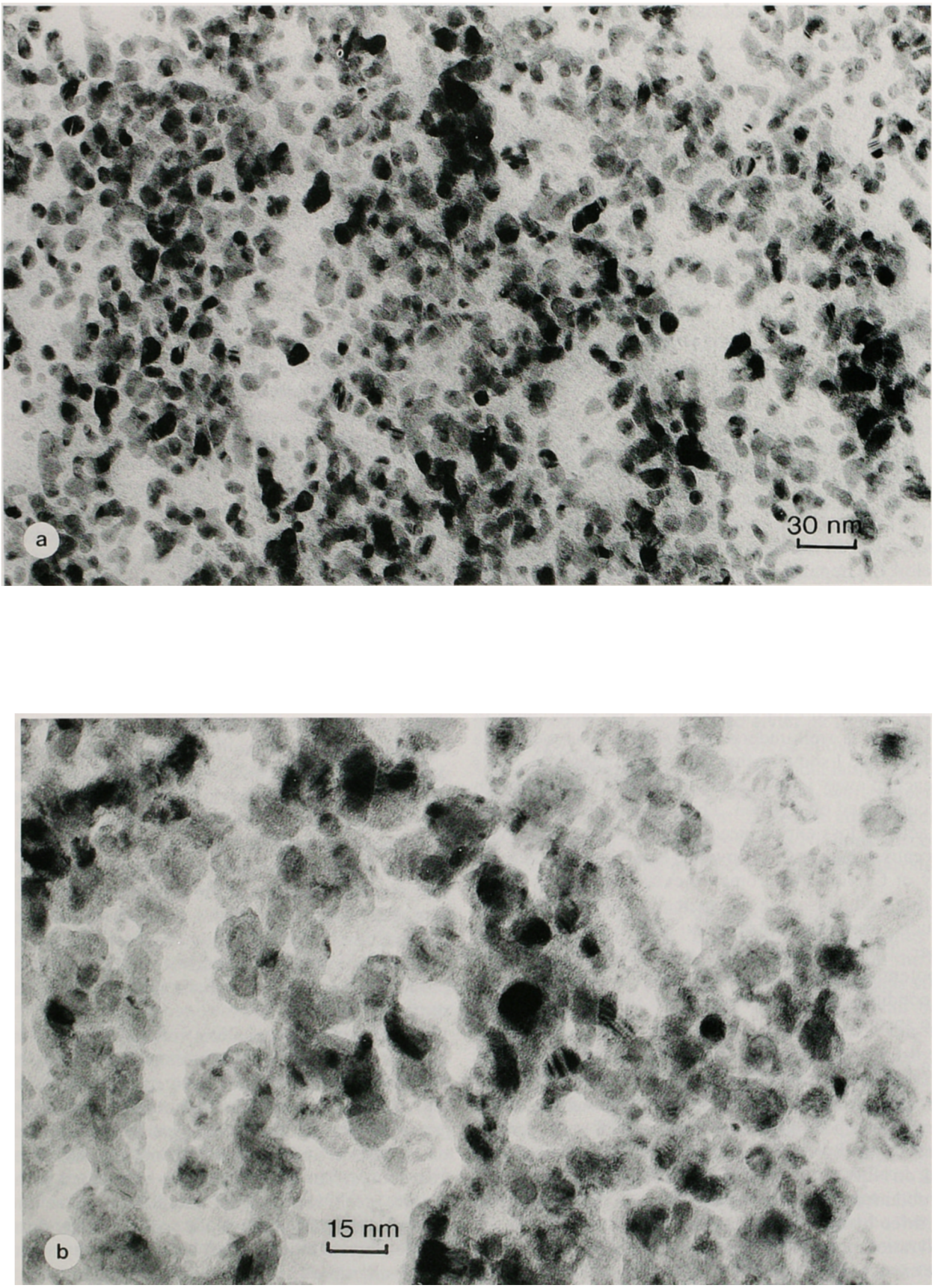

FIG. 6. TEM views at different magnifications of ultramicrotome thin sections of RNiSn2 catalyst: (a) 320,000× and (b) 660,000×

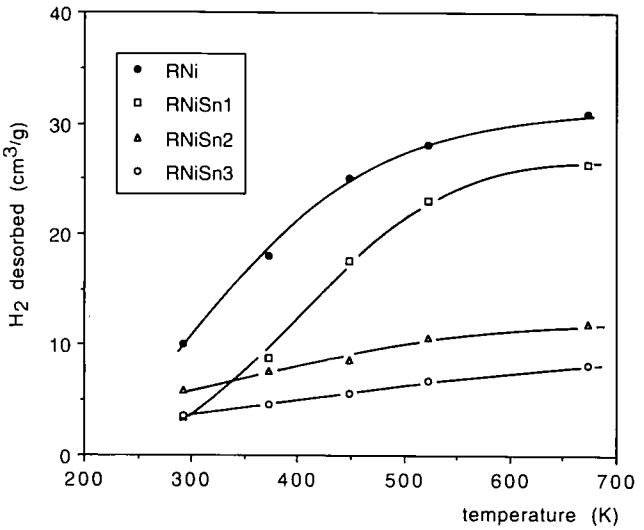

FIG. 7. Volume of dihydrogen thermodesorbed from the fresh catalysts.

shows that under reaction conditions tin is oxidized into insoluble SnO or $Sn(OH)_2$.

6.2. Activity and stability of catalysts. Table 2 indicates that the initial rates of glucose hydrogenation on the fresh Sn-promoted catalysts are always much higher than that on the base catalyst RNi. Thus, a fivefold rate enhancement is observed with catalyst RNiSn3. The effect is interpreted in the same way as in the case of Raney-nickel catalysts containing Mo, Cr and Fe. Indeed, under reaction conditions all these elements are in an oxidized form on the nickel surface and they can activate the C=O bond hydrogenation as described previously.

However, the catalysts deactivate very rapidly; thus, on the third hydrogenation run with RNiSn3 the rate is 16 times smaller than on the fresh catalyst and 3 times smaller than on RNi. Figure 5 shows that the deactivation is by far the largest among the different catalysts investigated. The mechanism of deactivation is basically similar to that of Fe-promoted catalysts, namely tin atoms are removed from the surface and no longer promote activation of the C=O group. However, the deactivation of Sn-promoted catalyst is worse because as shown by STEM-EDX study oxidized tin species remain in the vicinity of the nickel crystallites, probably in the form of hydroxide $Sn(OH)_2$ which blocks the micropores and thus the access to the nickel surface.

CONCLUSIONS

This study brings new data on the effect of chromium, molybdenum, iron and tin on the activity of Raney-nickel catalysts in glucose hydrogenation and a mechanism of action of these promoters is proposed. More specifically the following points are highlighted.

1. A homogeneous distribution of promoter atoms in the Raney-nickel grain is required to produce a large rate enhancement. This can be obtained by starting from a precursor alloy where the metal promoters are already homogeneously associated with the nickel in the Ni_2Al_3 phase; otherwise, the promoter is either leached away during the soda attack or it agglomerates into inactive deposit. Furthermore, tin loading via controlled surface reaction of $Sn(Bu)_4$ with hydrogen atoms on the surface is a very efficient way to cover the Raney-nickel surface with tin atoms. The amount of tin fixed is controlled easily and its distribution in the Raney-nickel grain is homogeneous on a nanometer scale.

2. The concentration of the promoter in the catalyst should not be too high, otherwise too many active nickel atoms will be covered. In the case of chromium and molybdenum promoted catalysts, an optimum concentration is obtained for a ratio M/Ni = 0.025. Assuming that all the Cr and Mo atoms are on the surface, a rough calculation indicates that 20 ± 10% of the surface would be occupied by these atoms. Interestingly, a similar surface concentration of promoter atoms M in Pt–M (M = Fe, Ru) catalysts was also found to be optimum to obtain the highest rate of C=O hydrogenation of unsaturated aldehydes (29–31).

3. Under the reaction conditions the catalyst is at a potential where chromium surface atoms are in the Cr^{III} oxidation state. The rate enhancement can be interpreted with a mechanism of activation and hydrogenation of the C=O bond similar to that proposed earlier for aldehydes (30, 31), namely, the C=O bond is polarized by donation of a lone electron pair of the oxygen to surface Cr^{III} species acting as Lewis acid sites. This polarization favours the nucleophilic attack of the carbon by hydrogen dissociatively adsorbed on nickel. This mechanism implies a good distribution and an optimum concentration of the metal promoter, as discussed in points 1 and 2 above. It should apply for any electropositive promoters like chromium, molybdenum, iron, and tin.

4. The aging of molybdenum and chromium-promoted catalysts after five recyclings is due in small part to a weak sintering of the sponge metal but it is mainly due to the poisoning of the active sites by organic fragments formed via side reactions, e.g., cracking products. However, this deactivation is not representative of the aging of catalysts after many recyclings under industrial operation where metal sintering could well be the major cause of deactivation. On the other hand, iron- and tin-promoted catalysts deactivate very rapidly because the promoters are leached away from the surface. The deactivation of tin-containing catalyst is even worse

because tin hydroxide remains in the micropores and hinders the diffusion and adsorption of glucose on the nickel surface.

REFERENCES

1. Montgomery, S. R., *in* "Catalysts of Organic Reactions" (W. R. Moser, Ed.), p. 383, Dekker, New York, 1981.
2. Fouilloux, P., *Appl. Catal.* **8,** 1 (1983).
3. Hadley, R. I., U.S. Patent 2,948,687 (1960).
4. Court, J., Damon, J. P., Masson, J. and Wiezchowski, P., *in* "Heterogeneous Catalysis and Fine Chemicals" (M. Guisnet, J., Barrault, C. Bouchoule, D. Duprez, C. Montassier, and G. Perot, Eds.), p. 189. Elsevier, Amsterdam, 1988.
5. Bizhanov, F. B., Sokolskii, D. W., Nadirov, N. K., and Khandodzhaev, Sh., *Kinet. Katal.* **12,** 217 (1971).
6. Shcheglov, N. I. and Sokolskii, D. V., *Trudy Inst. Khim. Nauk Akad. Nauk Kazakh. SSR* **5,** 92 (1959).
7. Bizhanov, F. B., U.S. Patent 4,018,835 (1977).
8. Azimbekova, R. A., Ivchenko, A. G., and Abidova, M. F., *Uzb. Khim. Zh.* **4,** 73 (1985).
9. Margitfalvi, J., Hegedüs, M., Göbölös, S., Kern-Tálas, E., Szedlacsek, P., and Szabó, S., *in* Proceedings, 8th International Congress on Catalysis. Berlin, 1984," Vol. 4, p. 903, Verlag-Chemie, Weinheim, 1984.
10. Travers, Ch., Bournonville, J. P., and Martino, G., *in* "Proceedings, 8th International Congress on Catalysis, Berlin, 1984," Vol. 4, p. 891. Verlag-Chemie, Weinheim, 1984.
11. Ferretti, O. A., Bettega de Paoli, L. C., Candy, J. P., Mabilon, G. and Bournonville, J. P. *in* "Preparation of Catalysts. IV. Scientific Bases for the Preparation of Heterogeneous Catalysts" (B. Delmon *et al.*, Eds.), p. 712. Elsevier, Amsterdam, 1987.
12. Candy, J. P., Ferretti, O. A., Mabilon, G., Bournonville, J. P., El Mansour, A., Basset, J. M., and Martino, G., *J. Catal.* **112,** 210 (1988).
13. Bournonville, J. P., Candy, J. P., and Mabilon, G., U.S. Patent 4,628,130 (1986).
14. Margitfalvi, J. L., Göbölös, S., Tálas, E., and Hegedüs, M., *in* "Preparation of Catalysts V" (G. Poncelet, P. A. Jacobs, P. Grange, and B. Delmon, Eds.), p. 669. Elsevier Amsterdam, 1991.
15. Cerino, P. J., Flèche, G., Gallezot, P. and Salome, J. P., *in* "Heterogeneous Catalysis and Fine Chemicals II" (M. Guisnet, J. Barrault, C. Boulouche, D. Duprez, G. Perot, R. Maurel, and C. Montassier, Eds.), p. 231. Elsevier, Amsterdam, 1991.
16. Klug, H. P., Alexander, L. E., "X-Ray Diffraction Procedures." Wiley, New York, 1974.
17. Fouilloux, P., Martin, G. A., Renouprez, A. J., Moraweck, B., Imelik, B., and Prettre, M., *J. Catal.* **25,** 212 (1972).
18. Brahme, P. H., Pai, M. V., and Narsimhan, G., *Brit. Chem. Eng.* **9,** 684 (1964).
19. Wisniak, J., and Simon, R., *Ind. Eng. Chem. Prod. Res. Dev.* **15,** 130 (1979).
20. Chang, F. W., Kuo, K. T., and Lee, C. N., *J. Chin. Inorg. Chem. Eng.* **12,** 167 (1981).
21. Brahme, P. H., and Doraiswamy, L. K., *Ind. Eng. Chem. Prod. Res. Dev.* **18,** 50 (1979).
22. Sachtler, W. M. H., and Fahrenfort, J., *in* "Proceedings, 2nd International Congress on Catalysis, Paris, 1960," p. 831, Technip, Paris, 1961.
23. Selwood, P. W., "Chemisorption and Magnetization," Academic Press, New York, 1975.
24. Kaufman, L., and Nesor, H., *Metall. Trans.* **5,** 1623 (1974).
25. Bonnier, J. M., Damon, J. P., and Masson, J., *Appl. Catal.* **42,** 285 (1988).
26. Bonnier, J. M., Damon, J. P., Delmon, B., Doumain, B., and Masson, J., *J. Chim. Phys.* **84,** 889 (1987).
27. Khaidar, M., Allibert, Ch., and Dride, J., *Z. Metall.* **7,** 433 (1982).
28. Tri, T. M. Candy, J. P., Gallezot, P., Massardier, J., Primet, M., Védrine, J. C., and Imelik, B., *J. Catal.* **79,** 396 (1983).
29. Goupil, D., Fouilloux, P., and Maurel, R., *React. Kinet. Catal. Lett.* **35,** 185 (1985).
30. Richard, D., Ockelford, J., Giroir-Fendler, A., and Gallezot, P., *Catal. Lett.* **3,** 53 (1989).
31. Gallezot, P., Giroir-Fendler, A., and Richard, D., *in* "Catalysis of organic reactions" (W. E. Pascoe, Ed.), p. 1. Dekker, New York, 1992.